IEEE Access
Multidisciplinary | Rapid Review | Open Access Journal

Received April 19, 2019, accepted May 7, 2019, date of publication May 13, 2019, date of current version May 23, 2019.

Digital Object Identifier 10.1109/ACCESS.2019.2916411

Polar Expression Feature of Digitized Handwritten Pattern for Automated-Parkinson's-Disease Screening Using Perceptual Color Representation-Based Classifier

PING-JU KAN[1,2], CHIA-HUNG LIN[3], CHEN-SAN SU[4], HSIN-YU LIN[1], WEI-LING CHEN[1], AND CHIH-KUANG LIANG[5]

[1]KSVGH Originals and Enterprises, Kaohsiung Veterans General Hospital, Kaohsiung 81362, Taiwan
[2]Department of Computer Science, University of Toronto, Toronto, ON M5S 1A1, Canada
[3]Department of Electrical Engineering and Artificial Intelligence Application Research Center, National Chin-Yi University of Technology, Taichung 41170, Taiwan
[4]Division of Neurology, Kaohsiung Veterans General Hospital, Kaohsiung 81362, Taiwan
[5]Center for Geriatrics and Gerontology, Kaohsiung Veterans General Hospital, Kaohsiung 81362, Taiwan

Corresponding authors: Chih-Kuang Liang (ckliang@vghks.gov.tw) and Chia-Hung Lin (eechl53@gmail.com)

ABSTRACT Functional tremors are clear symptoms of neurodegenerative diseases; as such, they indicate the progression of Parkinson's disease (PD). Digitized handwritten pattern analysis of Archimedes' spirals, words, and sentences can help evaluate movement discords in the upper limbs. It offers a simple, comfortable, and repeatable method of examination for clinical applications and at-home monitoring usages. Upper limb tremors can be found in PD, essential tremor (ET), and cerebellar disorders. This paper proposes a quantitative method to scale the variations of functional tremors. The deviation (in cm) and the accumulation angle (in rad) of the feature pattern in polar expression were extracted to scale the variability at different tremor levels. Then, the proposed intelligent classifier, which is used as a perceptual color representation-based classifier (PCRC) and comprises a radial Bayesian network and a color relation analysis method, was employed to screen PD or ET with perceptual color representation. An assistant tool can integrate a smart mobile device (iPad/smartphone) and PCRC into the decision support system for individualized functions to evaluate the progression of the tremor level. The proposed decision support system was validated using data collected from 50 subjects. With fivefold cross-validation, average true positive, average true negative, and hit rates of 92.02%, 88.17%, and 90.44%, respectively, were obtained to quantify the performance of the proposed classifier for identifying normal controls and PD or ET.

INDEX TERMS Parkinson's diseases, deviation, accumulation angle, radial Bayesian network, perceptual color representation- based classifier.

I. INTRODUCTION

Parkinson's disease (PD) is a chronic and long-term neurodegenerative disease that gradually affects the motor system. Alzheimer's disease and neurodegenerative disorder lead to dementia and cognitive and behavioral problems. Patients with Parkinsonian and Alzheimer's diseases are the largest groups of those with neurode-generative disorders. These diseases can be caused by genetic and environmental factors. Their prevalence rates increase with advancing age in both males and females, and there is a tendency to develop at over ages greater than 60 years [1]–[3]. The main motor symptoms can be observed at an early stage of the disease, such as shaking, rigidity, slow movement, and walking difficulties, which are known as parkinsonisms. These symptoms slowly progress over time. PD features comprise physical signs such as muscular rigidity, rhythmic tremors, and postural instability. Tremors are involuntary rhythmic

The associate editor coordinating the review of this manuscript and approving it for publication was Alberto Cano.

2169-3536 © 2019 IEEE. Translations and content mining are permitted for academic research only.
Personal use is also permitted, but republication/redistribution requires IEEE permission.
See http://www.ieee.org/publications_standards/publications/rights/index.html for more information.

oscillations of the hands, arms, or legs (mostly occurring in the hands). These tremor symptoms have particular characteristics such as different frequencies, regularity/irregularity, and directionality. Essential tremor (ET) is a slowly progressive monosymptomatic disorder and starts on one side of the body and extends to affect both sides within 3 years; it tends to relapse at ages over 40 years. It involves rhythmic oscillation with high characteristic frequencies of 8–10 Hz (between 4 and 12 Hz) and postural tremors [4]. The characteristic frequencies decrease with age. PD tremor types include resting, postural, and action tremors, and the frequency band 4–6Hz is associated with the PD resting tremor. Tremors are a functional movement disorder that can be observed when the upper limbs are moving during limb stretching, writing, or drawing [7]–[9]. The tremors can be regular or irregular in amplitude and have a specific range of characteristic frequencies. Measurements of oscillation amplitudes, dominant frequencies, and directions with rhythmic or arrhythmic movements can help to confirm the presence of functional movement disorders.

As described in the literature [5], [6], [10]–[12], sensor-based quantitative methods, such as using a tri-axial accelerometer, tri-axial gyroscope, tri-axial magnetometer, laser-based displacement transducer, and electromyography, have been established to evaluate tremor levels and abnormal movements. These methods, with sensors worn on the subject's body (bilateral wrists and legs, waist, chest), are used to monitor motor dysfunction and to quantify bradykinesia, rigidity, and various types of tremors in PD patients [5], [12]. However, when using sensor-based quantitative methods, it is not possible to immediately observe the testing results. The aforementioned methods require the analysis of several features from the recorded signals via time-domain and frequency-domain analyses, including signal preprocessing, feature extraction, and pattern recognition and assessment. In analysis through signal preprocessing, bandpass filters are used to retain the desired frequency ranges, permitting the identification of the typical frequencies of tremors, including a bandpass filter at 3–6 Hz, 6–9 Hz, and 9–12 Hz for PD or resting tremor, ET or postural tremor, and kinetic tremor, respectively [5], [6], [10], [12]. In addition, the lengths of the data stream affect the resolution of tremor detection for analyzing different dominant frequency tremors.

Sensor-based methods with multiple channels (transition protocol) need to synchronously transmit sampling data from the sensors. Many acquired signals need to be analyzed. Patients must wear many wearable sensors, resulting in discomfort and limitations for at-home practical applications. After frequency-feature extraction, low-, medium-, and high-frequency tremors are divided into three groups for classification. Then, machine learning methods, such as the hidden Markov model, Bayes classification, support vector machine, and logistic regression, are selected to implement a decision support system for tremor classification [7], [13]–[15]. However, for complicated feature patterns, linear classification methods have difficulty solving nonlinear separable classification problems. Non-linear classifier-based pattern recognition systems, such as machine learning methods and support vector machine (SVM) with multi-layers [16]–[18], can solve nonlinear separable classification problems by identifying a nonlinear hyperplane in feature space. These methods have an average accuracy of 70%–90% in terms of identifying normal controls and PD or ET. The results of these methods indicate that the nonlinear SVM-based classifier performs better than the traditional neural networks [18]. The parameters of the kernel functions of the nonlinear SVM are required for optimization by the optimization algorithms with iterative computations for updating the network parameters. Moreover, determining the structure of the multilayer network and updating the parameters with iterative computations are the primary concerns. In clinical applications, it is essential to establish a simple assistant tool that can rapidly produce screening results through which neurologists can evaluate disease evolution with the effectiveness of drug treatment. Additionally, patients need a simple tool for at-home use for home-based monitoring.

Digitized handwritten patterns, including Archimedes' spirals, words, and sentences [5], [7], [15], [19]–[21], offer a computer-assisted tool to evaluate patients' symptoms in the shortest possible time. Computerized pattern analysis using an iPad, smartphone, or digital tablet with an Apple pencil or an ink-pen (pressure sensor) [5], [15] is a method of recording the dynamics when a patient draws a pattern or writes something. Its assistant tool can immediately acquire the digitized handwritten patterns in real time using customized software [7]. Therefore, the recording of the raw data of handwritten patterns via a smart mobile device (Apple, 12.9-inch iPad) and an intelligent classifier implement can be integrated into an assistant tool for home monitoring use. It can provide a comfortable writing/drawing tool for subjects under repeated examinations. In this study, a five-turn Archimedes' spiral and a 15-cm straight line were selected to evaluate the patients' symptoms. A spiral in polar coordinates is a straight line that can be easily compared with the handwritten spiral in the same coordinate. In digitized handwritten patterns, increased variability in amplitudes and frequencies can appear when drawing a pattern if a functional tremor occurs. To quantify the variations of functional tremors, the deviation (Dev, cm) and the accumulated angle (Θ, rad) of the feature pattern in polar coordinates are extracted to scale the variability at different tremor levels. Two key indices are parameterized using fuzzy membership functions with certainty grades between 0 and 1 [21], [22]. Then, for nonlinear separable classification, a nonlinear pattern-recognition scheme comprising a radial Bayesian network and the color relation analysis method is used to separate the normal control from PD or ET, [23]–[26], the so-called perceptual color representation-based classifier (PCRC). A radial Bayesian network with nonlinear membership functions can be conducted by a multi-layer pattern mechanism using nonlinear units to deal with nonlinear separable tasks. Hence, its pattern

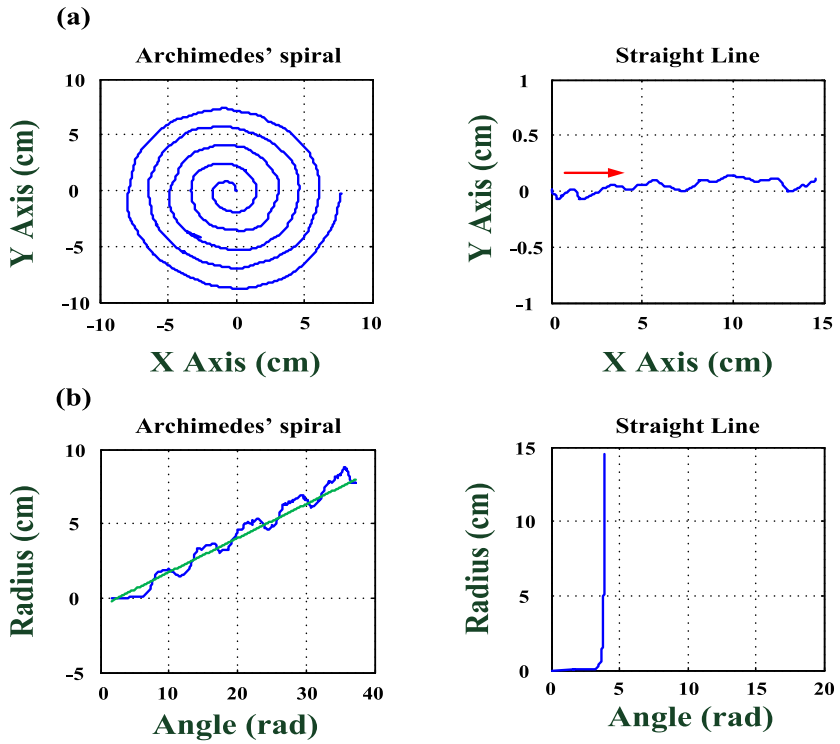

FIGURE 1. Sample Archimedes' spiral and straight line drawn on an iPad. (a) Sample drawn in the Cartesian coordinate system (normal control). (b) Polar representation of the radius (in cm) and angle (in rad) transformation.

mechanism separates the output values of a Bayesian network into "hue angle" and "saturation value" to screen PD or ET. In contrast to conventional intelligent classifiers, the proposed PCRC method is an automatic analytical tool without iterative computations, an optimization technique, parameter adjustment, or an inference scheme [25], [26]. The tremor levels are parameterized into the specific membership grades to describe normal controls, subjects with PD, and subjects with ET using the fuzzification operations. Its algorithm permits operation in a flexible manner with less parameter assignment. The PCRC method provides visual representation with color codes to realize PD screening, such as green series color for healthy subjects, blue series color for those with ET, and red series color for subjects with PD. Its algorithm is also easy to program using a laptop or a portable smart device. The experimental results will reveal the feasibility of automated screening for PD or ET.

The remainder of this article is organized as follows: Section II describes the methodology, including the handwritten spiral collection and analysis, and PCRC method. Section III presents decision support system implementation, tremor quantification and evaluation, and comparison with the conventional intelligent classifier. Section IV presents the experimental results and conclusions.

II. METHODOLOGY

A. HANDWRITTEN PATTERN COLLECTION AND ANALYSIS

Handwritten spirals (Archimedes' spirals) and straight lines were collected on an iPad (Apple, 12.9-inch iPad Pro, 120 Hz sampling rate) with an Apple pencil (240 Hz sampling rate, precision $\pm$ 0.25 mm) [5], [7], [15], [18]. As seen in Figure 1, subjects were asked to sit in a chair and draw two samples, including an Archimedes' spiral and a straight line, using their dominant hand. The handwritten samples were obtained in line with the following standard procedure:

- Record the Cartesian coordinates (x, y) with the variables, x_n and y_n, corresponding to the nth samples, $n = 1, 2, 3, \ldots$;
- Record the pen pressure applied by an Apple pencil in arbitrary units;
- Record the sampling number, N.

Each Archimedes' spiral was drawn from its center (original point) to its extremity (five turns anticlockwise) in a 10 cm $\times$ 10 cm square by the subjects, as seen in Figure 1(a). For the second sample, each subject drew a straight line from the left- to the right-hand side. The subjects were asked to draw each sample at their natural speed with no time limitation for sketching the guided spiral and the straight line. For two repeated measurements at each visit, the subjects drew two spiral samples and two straight lines with their dominant hand while the drawing arm was unsupported. The pressure sensor of the iPad was used to monitor whether the subject (she or he) drew the patterns. In this study, 100 spiral samples and 100 line samples were collected from 50 subjects, including normal control subjects, Parkinson's disease (PD) patients, and essential tremor (ET) patients, and analyzed. After the sampling coordinate points had been acquired,

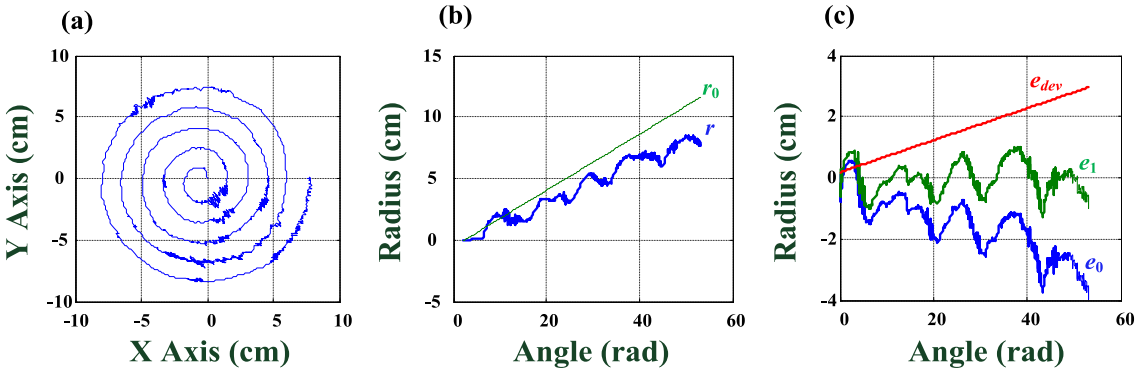

FIGURE 2. Linearized spiral trace (PD case). (a) Spiral trace in Cartesian coordinate system. (b) Spiral trace in polar representation. (c) Functional tremor quantification for a handwritten spiral.

the polar expression was used to linearize the traced spirals and straight lines by plotting the graph of radius (r) versus angle (θ), which are derived from the Cartesian coordinates to polar coordinates from the Apple pencil in the traced samples. r and θ are calculated as described previously [14], [19], [20]:

$$r_n = \sqrt{(x_n - x_0)^2 + (y_n - y_0)^2} \tag{1}$$

$$\theta_n = \tan^{-1}\left(\frac{y_n - y_0}{x_n - x_0}\right) \tag{2}$$

where coordinates x_0 and y_0 are the original point. Angle θ_n is returned as a series of increasing or decreasing positive or negative values in the Cartesian quadrant. The angles are calculated in the active quadrant using the change in sign and value of angle θ_n, and subsequently accumulating the radian angle from the previous iteration, as seen in the polar representation, $r_n \angle \theta_n, n = 1, 2, 3, \ldots, N$, in Figure 1 (b). The total accumulation angle, Θ, can be calculated as follows:

$$\Theta = \sum_{n=1}^{N-1} (\theta_{n+1} - \theta_n) \tag{3}$$

The pseudocodes for replacing the coordinate system are shown in the Appendix.

In this study, polar representations are used to analyze the crucial aspects of the drawn samples, as seen for the spiral trace and linearized spiral trace in Figures 2(a) and 2(b). While comparing the ideal template obtained through radius-angular transformation, the goal is to detect differences between the ideal template, r_{0n}, and traced sample, r_n. For estimating the tremor activity, the difference, e_{0n}, can be calculated as follows:

$$e_{0n} = abs(r_n - r_{0n}) \tag{4}$$

$$r_{0n} = \frac{8}{35}(\theta_n - 2.5) \tag{5}$$

where n is the sampling number, $n = 1, 2, 3, \ldots, N$; operator $abs(\cdot)$ is returned as the absolute value. The deviation curve, e_{dev}, is computed from the linearized spiral trace as follows:

$$e_{dev} = abs(e_0 - \text{detrend}(e_0)) = abs(e_0 - e_1) \tag{6}$$

where operator det*rend*$(\cdot)$ is a function of the detrending process used to remove the variations [27]–[29]. In clinical evaluation, a physiological assessment of a functional tremor is performed by assessing the increased variability of tremor amplitude and frequency during spiral drawing. To quantify the effect of the functional tremor, the deviation (Dev, cm) is employed to scale the increased variability with the accumulation angle, Θ', as follows:

$$Dev = \frac{abs(e_{dev,1} - e_{dev,N-1})\Theta'}{\Theta} = slope\Theta' \tag{7}$$

where Θ is the total accumulation angle. Index *Dev* is proportional to the accumulation angle, Θ'. Spiral is associated with the accumulation angle; hence, the fluctuation of the drawn spiral can be captured. As seen in Figure 3, spiral traces and linearized spiral traces indicate differences in a normal control subject (green line) and a PD subject (blue line). Hence, index *Dev* is used to separate the normal condition from PD and ET for handwritten spiral analysis. In addition, functional tremors indicate the variances in tremor amplitude and frequency during the drawing of a straight line. Owing to a lack of fluency in drawing the straight line, subjects are unable to complete the task quickly. Thus, the accumulation angle, Θ', increases as tremor amplitude and frequency increase in the polar representation, as seen in the normal control subject, and PD and ET subjects in Figure 4. The total accumulation angle, Θ, is selected to quantify the changes in movement characteristics, tremor amplitude, and tremor frequency using equation (3).

B. PERCEPTUAL COLOR REPRESENTATION-BASED CLASSIFIER (PCRC)

A total of 100 spiral samples and 100 line samples were collected and analyzed from normal control subjects (24), patients with PD (21), and patients with ET (5). Further, the collection of the raw data was approved by the hospital research ethics committee and the Institutional Review Board, under approval number VGHKS18-CT7-07#. For 100 pairs of feature parameters (*Dev*, Θ), 45 pairs of feature parameters (45% training patterns) were randomly selected

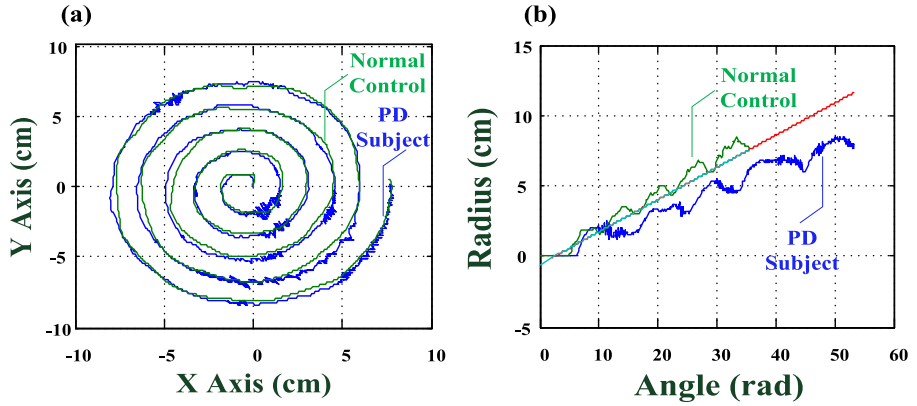

FIGURE 3. Characteristic comparisons for normal control and PD subjects. (a) Comparisons of spiral traces for normal control and PD subjects. (b) Comparisons of linearized spiral traces for normal control and PD subjects.

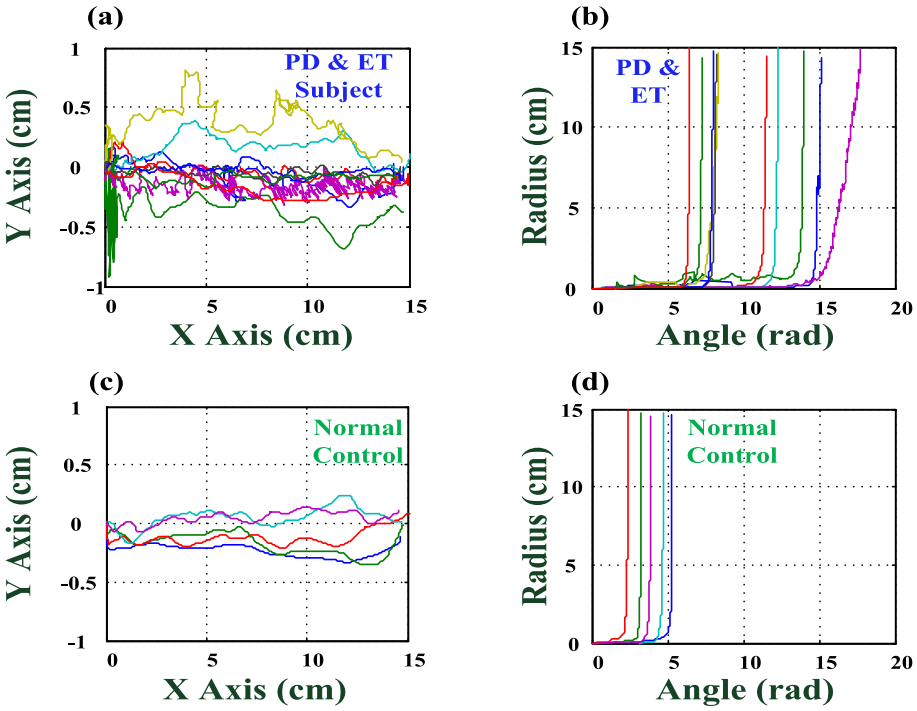

FIGURE 4. Movement characteristics in straight-line drawing. (a) Straight-line trace in Cartesian coordinate system for PD and ET subjects. (b) Straight line trace in polar representation for PD and ET subjects. (c) Straight line trace in Cartesian coordinate system for normal control subjects. (d) Straight line trace in polar representation for normal control subjects.

to train the PCRC classifier in the learning stage, and the remaining 55 pairs (55% testing patterns) were used to evaluate the PCRC classifier in recalling stage. The statistics for average deviations (cm), average accumulation angles (rad), and their standard deviations obtained using the 45 pairs of feature parameters are shown in Figure 5. According to Figure 5, two indices, *Dev* (cm) and Θ (rad), are parameterized with Gaussian, *Z* sigmoidal, and *S* sigmoidal membership functions, varying between values of 0 and 1 [22]–[24]. The value of certainty grades (CG) can be parameterized in specific ranges using equations (8)–(10), as follows:

- Membership functions, $\mu_{Dev,Nor}$, $\mu_{Dev,ET}$, and $\mu_{Dev,PD}$, can be used for parameterizing the index *Dev* (in cm) to describe the normal control, PD, and ET, as follows:

$$\mu_{Dev,Nor} = \begin{cases} \exp(-\frac{1}{2} \times (\frac{Dev - Dev_{Nor}}{\sigma_{Dev,Nor}})^2), & Dev > Dev_{Nor} \\ 1, & Dev \leq Dev_{Nor}, \end{cases}$$
$$\mu_{Dev,Nor} \in [0, 1] \quad (8)$$

$$\mu_{Dev,ET} = \exp(-\frac{1}{2} \times (\frac{Dev - Dev_{ET}}{\sigma_{Dev,ET}})^2),$$
$$0.00 < Dev < Dev_{max}, \mu_{Dev,ET} \in [0, 1] \quad (9)$$

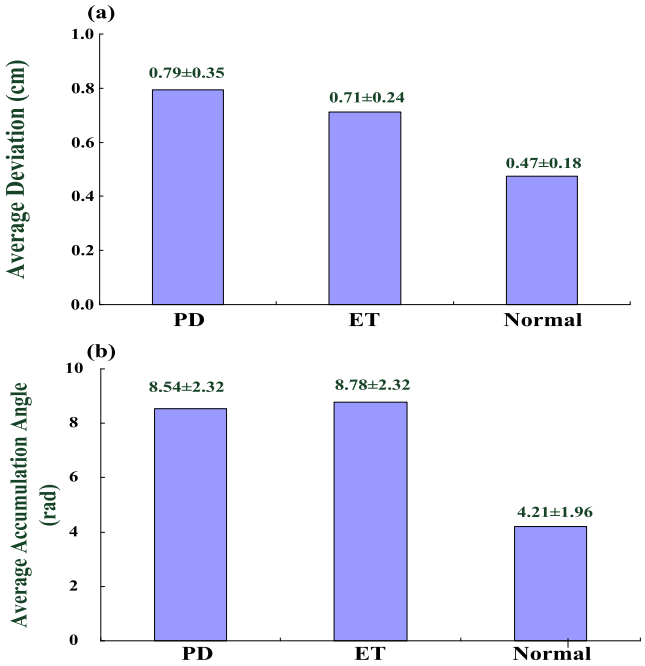

FIGURE 5. Statistics for average deviations (cm) and average accumulation angles (in rad). (a) Average deviations (in cm) for three conditions. (b) Average accumulation angle (rad) for three conditions.

$$\mu_{Dev,PD} = \begin{cases} \exp(-\frac{1}{2} \times (\frac{Dev - Dev_{PD}}{\sigma_{Dev,PD}})^2), & Dev < Dev_{PD} \\ 1, & Dev \geq Dev_{PD}, \end{cases}$$
$$\mu_{Dev,PD} \in [0, 1] \quad (10)$$

where mean values Dev_{Nor}, Dev_{ET}, and Dev_{PD} are 0.47, 0.71, and 0.79, respectively, while standard deviations, $\sigma_{Dev,Nor}$, $\sigma_{Dev,ET}$, and $\sigma_{Dev,PD}$ are 0.18, 0.24, and 0.35, respectively; $Dev_{max} = 2.00$ cm is the maximum deviation.

- Membership functions, $\mu_{Ang,Nor}$, $\mu_{Ang,ET}$, and $\mu_{Ang,PD}$, can be used for parameterizing the Θ (rad) to describe the normal control, PD, and ET, as follows:

$$\mu_{Ang,Nor} = \begin{cases} \exp(-\frac{1}{2} \times (\frac{\Theta - \Theta_{Nor}}{\sigma_{Ang,Nor}})^2), & \Theta > \Theta_{Nor} \\ 1, & \Theta \leq \Theta_{Nor}, \end{cases}$$
$$\mu_{Ang,Nor} \in [0, 1] \quad (11)$$
$$\mu_{Ang,ET} = \exp(-\frac{1}{2} \times (\frac{\Theta - \Theta_{ET}}{\Theta_{Ang,ET}})^2), 0.00 < \Theta < \Theta_{max},$$
$$\mu_{Ang,ET} \in [0, 1] \quad (12)$$
$$\mu_{Ang,PD} = \begin{cases} \exp(-\frac{1}{2} \times (\frac{\Theta - \Theta_{PD}}{\sigma_{Angv,PD}})^2), & \Theta < \Theta_{PD} \\ 1, & \Theta \geq \Theta_{PD} \end{cases},$$
$$\mu_{Ang,PD} \in [0, 1] \quad (13)$$

where mean values Θ_{Nor}, Θ_{ET}, and Θ_{PD} are 4.21, 8.78, and 8.54; while standard deviations, $\sigma_{Ang,Nor}$, $\sigma_{Ang,ET}$, and $\sigma_{Ang,PD}$ are 1.96, 2.32, and 2.32, respectively; and $\Theta_{max} = 20.00$ rad is the maximum accumulation angle. Then, a set of IF-THEN rules is used to represent linguistic inference rules, as follows:

$$\text{Rule 1\#: IF } (G_1 = \mu_{Dev,Nor} \text{ and } G_4 = \mu_{Ang,Nor}) \text{ THEN } y_1 \ (Normal\ Control) \quad (14)$$
$$\text{Rule 2\#: IF } (G_2 = \mu_{Dev,ET} \text{ and } G_5 = \mu_{Ang,ET}) \text{ THEN } y_2 \ (ET) \quad (15)$$
$$\text{Rule 3\#: IF } (G_3 = \mu_{Dev,PD} \text{ and } G_6 = \mu_{Ang,PD}) \text{ THEN } y_3 \ (PD) \quad (16)$$

where six certainty grades ($\mu_{Dev,Nor}$, $\mu_{Dev,ET}$, $\mu_{Dev,PD}$, $\mu_{Ang,Nor}$, $\mu_{Ang,ET}$, and $\mu_{Ang,PD}$) are propositions (G_1, G_2, G_3, G_4, G_5, and G_6); and y_1, y_2, and y_3 are the assigned classes. Then, a radial Bayesian network represents the output probabilistic relationships among the three classes ($m = 3$) as follows:

$$y_j = \sum_{k=1}^{6} w_{kj} G_k \Big/ \sum_{k=1}^{6} G_k \quad (17)$$
$$w_{kj} = \begin{cases} 1, & k \in Class\ j \\ 0, & k \notin Class\ j \end{cases}, \quad j = 1, 2, 3, \ k = 1, 2, 3, 4, 5, 6 \quad (18)$$

where the values of $w_{kj} \in [0, 1]$ assign the connection weights for the three classes, which are coded as binary values, encoding (1) *Class* 1 (Normal Control): [1, 0, 0, 1, 0, 0], (2) *Class* 2 (ET): [0, 1, 0, 0, 1, 0], and (3) *Class* 3 (PD): [0, 0, 1, 0, 0, 1], with a value of "1" for possible class, and all other classes are encoded with a "0" value. The connecting weights from the overall propositions to the summation node, ΣG_k, are set as 1. The associated nodes, y_1, y_2, and y_3, denote three classes: *Normal control*, *ET*, and *PD*. The Bayesian network computes the probabilities of the presence of three classes and subsequently transfers them to the gray grade for each class, $y_1 = g_1$, $y_2 = g_2$, and $y_3 = g_3$, as vector $g = [g_1, g_2, g_3]$. Then, the minimum and maximum gray grades are obtained as follows:

$$g_{\min} = \min[g_1, g_2, g_3] \quad (19)$$
$$g_{\max} = \max[g_1, g_2, g_3] \quad (20)$$

where $g_{\min} \neq g_{\max}$ (constraint condition). According to the HSV color model, with hue angle, angular dimension started at the red primary at 0° through green primary (120°) and blue primary (240°) and then back to red primary (360°). The model comprised neutral, achromatic, or gray colors, ranging from black (0) at lightness 0 to white (1) at lightness 1. The hue angle, $H \in [0, 360°]$, could be defined as follows [21], [22]:

$$H = \begin{cases} 60 \times (\frac{g_1 - g_2}{\Delta g}), & g_{\max} = g_3, g_1 \geq g_2 \\ 120 + 60 \times (\frac{g_2 - g_3}{\Delta g}), & g_{\max} = g_1 \\ 240 + 60 \times (\frac{g_3 - g_1}{\Delta g}), & g_{\max} = g_2 \\ 300 + 60 \times (\frac{g_2 - g_1}{\Delta g}), & g_{\max} = g_3, g_1 < g_2, \end{cases}$$
$$\Delta g = g_{\max} - g_{\min} \quad (21)$$

where $g_{min} = g_{max}$ and $H = 0$ (no geometric meaning). Index H, which refers to the three color series is used to identify the Normal Control, ET, and PD, as green series color (60°–180°), blue series color (180°–300°), and red series color (0°–60° or 300°–360°) in Figure 6. In addition, hue angle, H, is generally normalized to lie between 0 and 60, as follows:

$$h_c = \left[\frac{H}{6}\right], \quad h_c \in [0, 60] \tag{22}$$

where h_c is a suitable parameter for use in computer graphics applications and human user interfaces. The saturation, S, and value, V, are described as pure color saturation and lightness, respectively, which are defined as follows [24], [25]:

$$V = g_{\max} \quad , S = \begin{cases} 0, & g_{\max} = 0 \\ 1 - \dfrac{g_{\min}}{V}, & g_{\max} \neq 0 \end{cases} \tag{23}$$

These can help clinicians (expert neurologists) or patients to visualize the screening results. For tremor screening, index H is used to identify the three levels as angle points. An intelligent PCRC is conducted to automatically screen the possible tremor level, as shown in Figure 6(a). Subsequently, index S in the range 0.5–1.0 provides high confidence for confirming the possible level. Figure 6(b) shows the flowchart of Parkinson-related disease screening, including feature extraction, inference rules, and perceptual color representation-based classification.

C. DECISION SUPPORT SYSTEM IMPLEMENTATION

The proposed decision support system was implemented in a computer-assisted application program for Parkinson-related disease screening, as seen in the user interface in Figure 7(a). The screening algorithms, such as the feature extraction and PCRC algorithms, were established using the high-level, graphical, and text-based programming language in LabVIEW programming software and MATLAB workspace (NITM, Austin, TX, USA). These intelligent algorithms are the core techniques used to automatically extract the feature parameters and assess the signs from the handwritten templates. The data acquisition system comprised an iPad (Apple) and an Apple pencil. In this study, each subject had to draw a spiral sample and a straight line on the iPad screen using the Apple pencil. The digitized data were transferred to a laptop/PC for further analysis, as shown on the left-hand side of Figure 7(a), and to store the Cartesian coordinates of the drawing points over time in a two-dimensional (2D) area, as depicted in Figure 7(b). The PCRC was designed as a decision support method with two input variables (deviation and accumulation angle), six membership functions, three associated nodes, and one summation node in the Bayesian network. The outputs of associated nodes and summation node were used to circulate the probabilistic relationships among three classes. Then, PCRC utilized the output values of Bayesian network into ''hue angle'' and ''saturation value'' to identify the normal control, ET, or PD through perceptual color representation, including green, blue, and red series colors. The colormap function can be used to display the hue angle as colors in computer graphics applications and human user interfaces. The proposed decision support system was employed to automatically screen the signs in the handwritten templates to identify subjects potentially suffering from PD or ET. Hence, the integration of a portable data acquisition system and a decision support system was established to detect the progression of Parkinson-related diseases to aid neurologists in preliminary diagnosis and home-based monitoring. The goal here is to identify and warn subjects of impending illness as early as possible and to offer them appropriate treatment.

III. EXPERIMENTAL RESULTS

A. TREMOR QUANTIFICATION AND EVALUATION

Experimental data were obtained from 100 subjects; age range, 26–97 years; average age, 67.8 ± 14.1 years) enrolled at Kaohsiung Veterans General Hospital, Kaohsiung City, Taiwan, including normal controls (without tremor), those with PD, ET, dementia, and other tremor types (psychogenic, action, or postural tremors), as related profile in the Appendix. Tremors could be defined as rhythmic shaking or involuntary rhythmic movements in clinical indications. Subjects with PD exhibited physical signs such as muscular rigidity, rhythmic tremor, and postural instability. Symptoms associated with ET were rhythmic oscillation with high characteristic frequencies. For PD and ET investigations, subjects with dementia, subjects undergoing drug treatment, and erroneous measurements were excluded from the dataset. Tremors might occur in healthy subjects, the so-called physiological tremors. Such type of tremors was also excluded. Furthermore, subjects with PD or ET could potentially draw spiral and straight-line templates effectively. If their tremors were absent at the time of drawing, the subjects would be asked to resample. Thus, three datasets were selected to validate the proposed decision support system, including 24 normal control subjects, 21 patients with PD, and 5 patients with ET (as shown in the Appendix), with clinical measurement data and examinations with the proposed decision support system. Figure 8 shows the typical handwritten spiral templates drawn by PD and ET subjects (ET/postural tremor). It can be seen that the normal control subjects drew a regular spiral template. Those with ET tremors exhibited symmetrical and bilateral postural tremors with symptom frequencies between 4 and 12 Hz [4]. The findings demonstrated that the handwritten spiral template exhibited a regular fluctuation (saw-like pattern and harmonics) along the traced trajectory, as shown in Figure 8(a). Moreover, the frequencies of postural tremors were lower (between 4 and 9 Hz) than those of ET. The frequency distributions of ET and postural tremors overlapped in the range of symptom frequencies. Subjects with PD had lower symptom frequencies between 4 and 6 Hz [5]. Oscillatory movement involved a rhythmic back-and-forth action with the thumb and the index finger

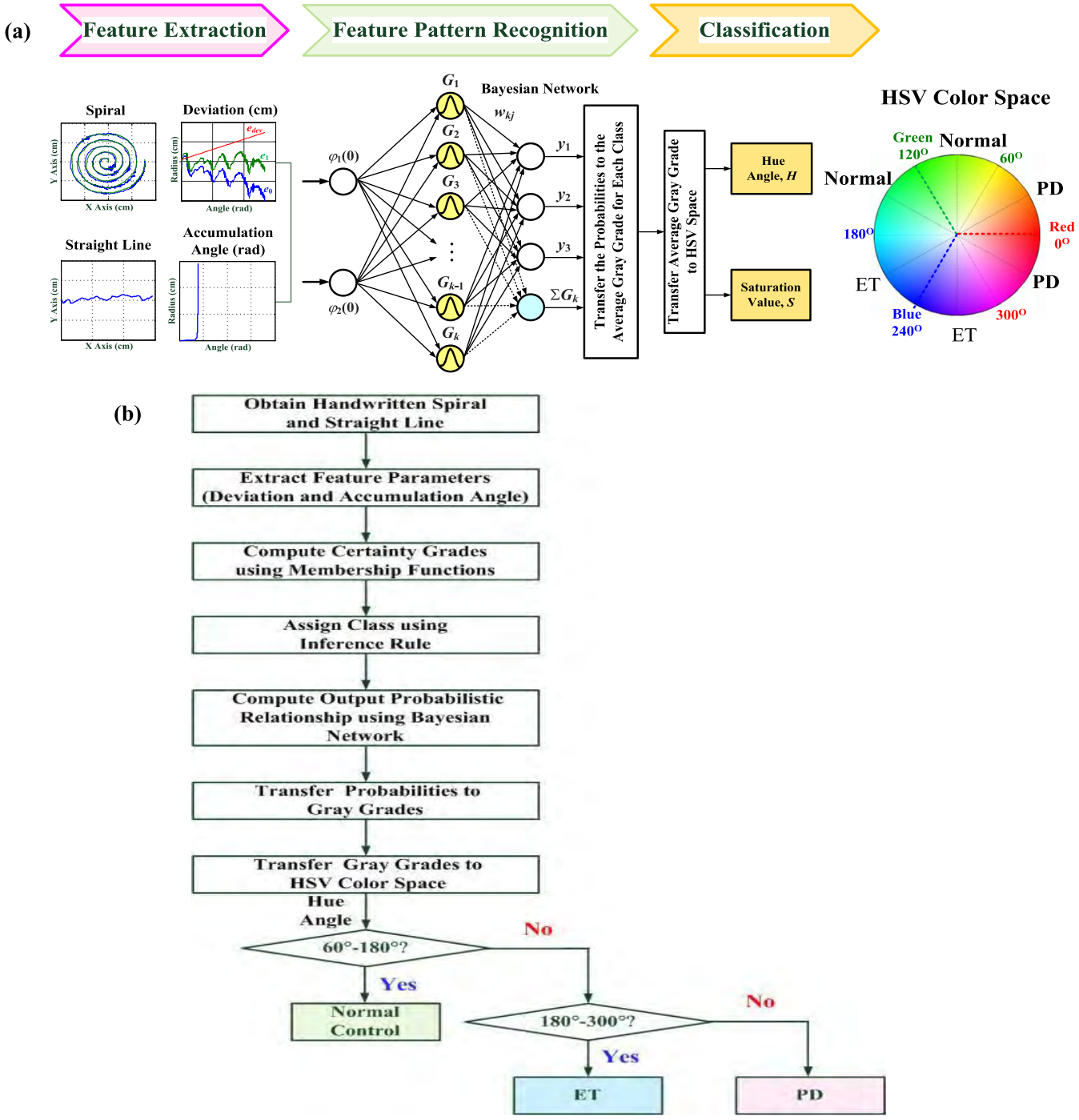

FIGURE 6. Decision support model. (a) The structure of intelligent classifier and perceptual color representation, (b) Flowchart of Parkinson related diseases screening.

(pill-rolling tremor) [6]. The spiral template presented a longer spiral and asymmetric arc, as depicted in Figure 8(b). In addition, approximately 60% of PD subjects experienced postural tremors [21], as shown in Figure 8(c). Moreover, regarding the characteristics of the straight line, it showed irregular fluctuation in amplitude and frequency for PD and ET cases, as depicted for subjects with PD and ET in Figure 4(a) and for normal controls in Figure 4(c).

To quantify the irregular fluctuation observed along the traced trajectory, the index *Dev* was employed to scale the variability for extracting the feature parameter in the traced spiral; it could be divided into three groups: (1) normal control: 0.0464–0.6795 cm (average: 0.4743 ± 0.1866 cm), (2) ET: 0.5119–1.0651 cm (average: 0.7131 ± 0.2495 cm), and (3) *PD*: 0.5009–2.1838 cm (average: 0.7882 ± 0.3499 cm). The slope of the deviation curve, e_{dev} (cm/rad),

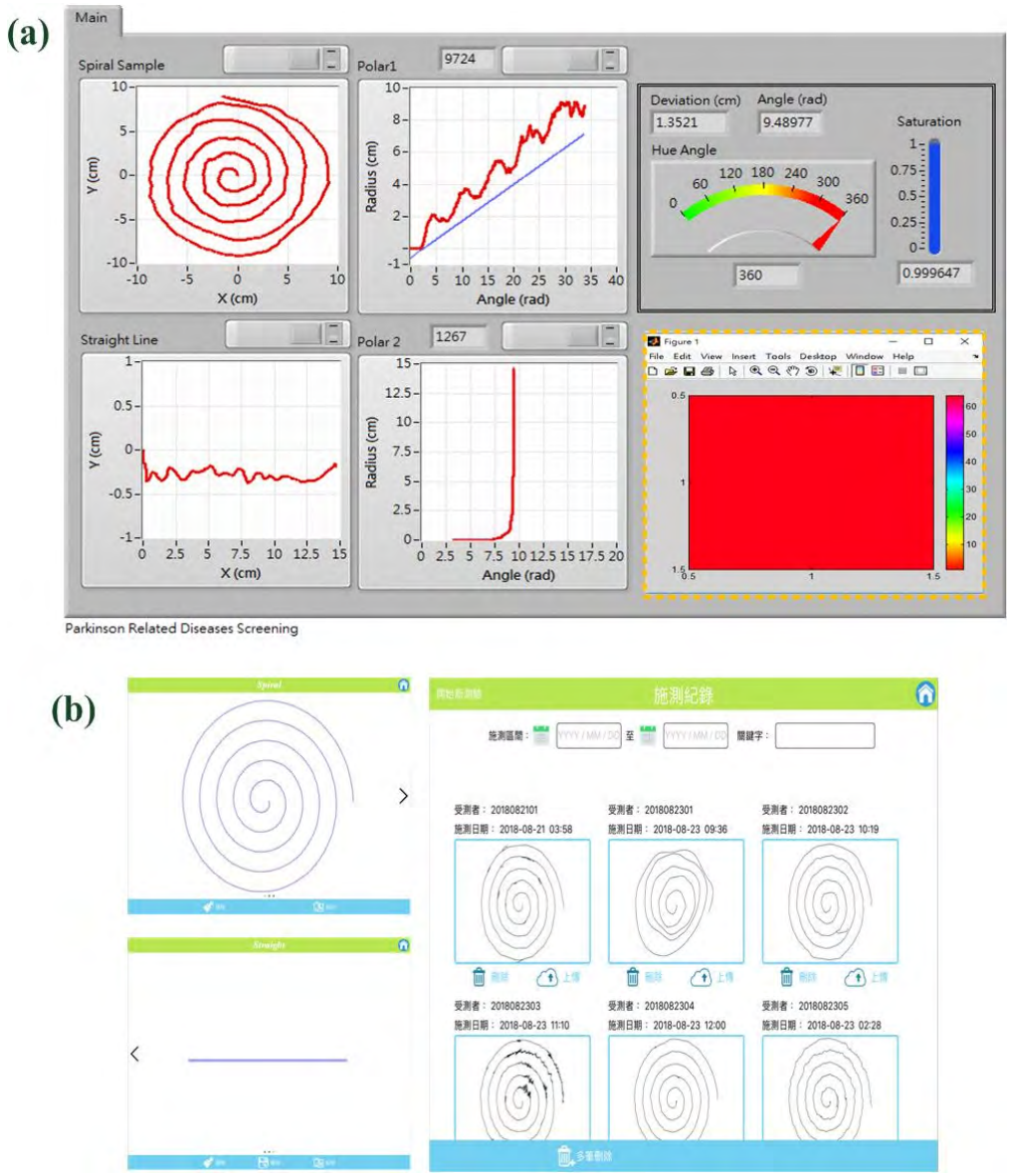

FIGURE 7. User interface for decision support system and data acquisition system. (a) Decision support system, (b) Data acquisition System.

increased as the tremor level increased in amplitude and frequency. The accumulation angle, Θ, was also used to quantify the variants for extracting the feature parameter in a traced straight line, as divided into three groups: (1) normal control: 2.0766–6.9883 rad (average: 4.21 ± 1.9681 rad), (2) *ET*: 5.9138–14.7004 (average: 8.7797 ± 2.3288 rad), and (3) *PD*: 5.5155–15.1349 rad (average: 8.5398 ± 2.3294 rad). The slope of the straight line trace in the polar representation decreased as the tremor level increased. These feature parameters were separated into specific ranges and used to separate the normal control from PD or ET as preliminary screening, which confirmed the utility of the feature parameters for further classification applications.

The experimental data obtained from participating subjects were randomly selected to verify the proposed decision support system in the recalling stage. The test data of 31 participating subjects are shown in Table 1. For example, subject #17 (aged 82 years), who had PD, exhibited rest, action, and postural tremors. Action and postural tremors appeared with rest tremors in the frequency distributions. Among these symptoms, action tremors occur in most PD cases. To quantify the irregular fluctuations, feature parameters were extracted from digitized handwritten spiral and straight-line templates using a feature extraction algorithm, as $Dev = 0.8154$ (cm) and $\Theta = 7.7541$ (rad), as seen in Table 1. The screening procedure for the decision support system was performed in line with the following procedure:

TABLE 1. Experimental results with feature parameters, *Dev* (cm) and Θ (rad) Note: Symbol ∗: Handedness, symbol L: Left hand side, and symbol R: Right hand side.

Subject No/Class		Age (*)	Parameter 1		Parameter 2		Expert Neurologist Decision	Proposed Method	
			Dev (cm)	Slope (cm/rad)	Θ (rad)	Slope (cm/rad)		*H*	*S*
1	Normal Control	70 (L)	0.4043	0.0102	3.8480	3.5062	Normal	123.14 (Green) Normal	0.9453
2		68 (R)	0.3857	0.0119	3.8038	4.1518	Normal	122.58 (Green) Normal	0.9556
3		78 (R)	0.5829	0.0164	4.8093	3.1521	Normal	133.71 (Green) Normal	0.8806
4		60 (L)	0.4886	0.0128	3.0548	4.7873	Normal	126.57 (Green) Normal	0.8806
5		97 (L)	0.4272	0.0131	3.9078	3.6946	Normal	123.91 (Green) Normal	0.9298
6		75 (R)	0.4067	0.0107	3.5694	4.0430	Normal	123.27 (Green) Normal	0.9473
7		54 (L)	0.6647	0.0186	3.3032	4.3849	Normal	141.06 (Green) Normal	0.4017
8		76 (R)	0.5356	0.0139	4.5867	3.2845	Normal	129.21 (Green) Normal	0.8075
9	ET	73 (R)	0.8379	0.0255	8.0693	1.7970	ET (Postural Tremor, Vocal Cord Tremor)	350.75 (Red) PD	0.9816
10		73 (R)	0.6693	0.0195	8.0491	1.7759	ET (Postural Tremor, Vocal Cord Tremor)	295.05 (Blue Violet) ET	0.8321
11		67 (L)	0.6541	0.0204	6.9356	2.1157	ET (Parkinsonism)	292.99 (Blue Violet) ET	0.6646
12		43 (R)	0.6754	0.0181	6.4714	2.3177	ET	293.45 (Blue Violet) ET	0.6031
13		80 (R)	0.8972	0.0253	3.4177	4.2690	ET (Postural Tremor)	359.47 (Red) PD	0.4552
14		43 (R)	0.7185	0.0229	5.9138	2.4748	ET	298.296 (Blue Violet) ET	0.4915
15	PD	74 (R)	0.7450	0.0213	12.6054	1.1467	PD	330.40 (Red) PD	0.9508
16		74 (R)	0.3924	0.0113	11.5562	1.2551	PD	352.84 (Red) PD	0.6181
17		82 (L)	0.8154	0.0234	7.7541	1.9210	PD (Resting Tremor)	351.97 (Red) PD	0.9666
18		79 (L)	1.4380	0.0487	3.5638	4.4143	PD (Dementia)	359.40 (Red) PD	0.9936
19		79 (R)	1.3527	0.0401	9.0498	1.8600	PD (Dementia)	329.58 (Red) PD	0.9989
20		77 (R)	0.5009	0.0134	13.2592	1.5238	PD (Action Tremor)	337.29 (Red) PD	0.6102
21		82 (R)	0.7317	0.0207	7.3233	1.9779	PD (Action and Rest Tremors)	358.38 (Red) PD	0.8822
22		69 (R)	0.7854	0.0222	12.3170	1.2255	PD (Tremor)	329.41 (Red) PD	0.9768
23		72 (L)	0.9116	0.0274	6.5306	2.2652	PD (Parkinsonism)	331.18 (Red) PD	0.8312
24		83 (L)	0.9388	0.0241	8.3402	1.7987	PD	341.06 (Red) PD	0.9935
25		56 (R)	0.7318	0.0224	6.3447	2.3055	PD (Severe Tremor)	357.96 (Red) PD	0.6858
26		83 (L)	0.4947	0.0127	12.2890	1.1813	PD (Parkinsonism)	337.13 (Red) PD	0.5603
27		69 (R)	0.6249	0.0167	8.2187	1.7740	PD (Parkinsonism)	291.11 (Blue violet) ET	0.7304
28		68 (R)	0.6574	0.0199	13.5540	1.0709	PD (Action and Rest Tremors)	326.66 (Red) PD	0.8072
29		82 (R)	0.7552	0.0219	8.9841	1.6551	PD (Parkinsonism)	359.26 (Red) PD	0.9577
30		64 (R)	0.7123	0.0203	4.9088	3.0705	PD (Pdism)	195.77 (Cyan) ET	0.0635
31		74 (L)	0.4779	0.0127	6.6229	2.1975	PD (Rest Tremor, Rigidity)	131.72 (Green) Normal	0.4123

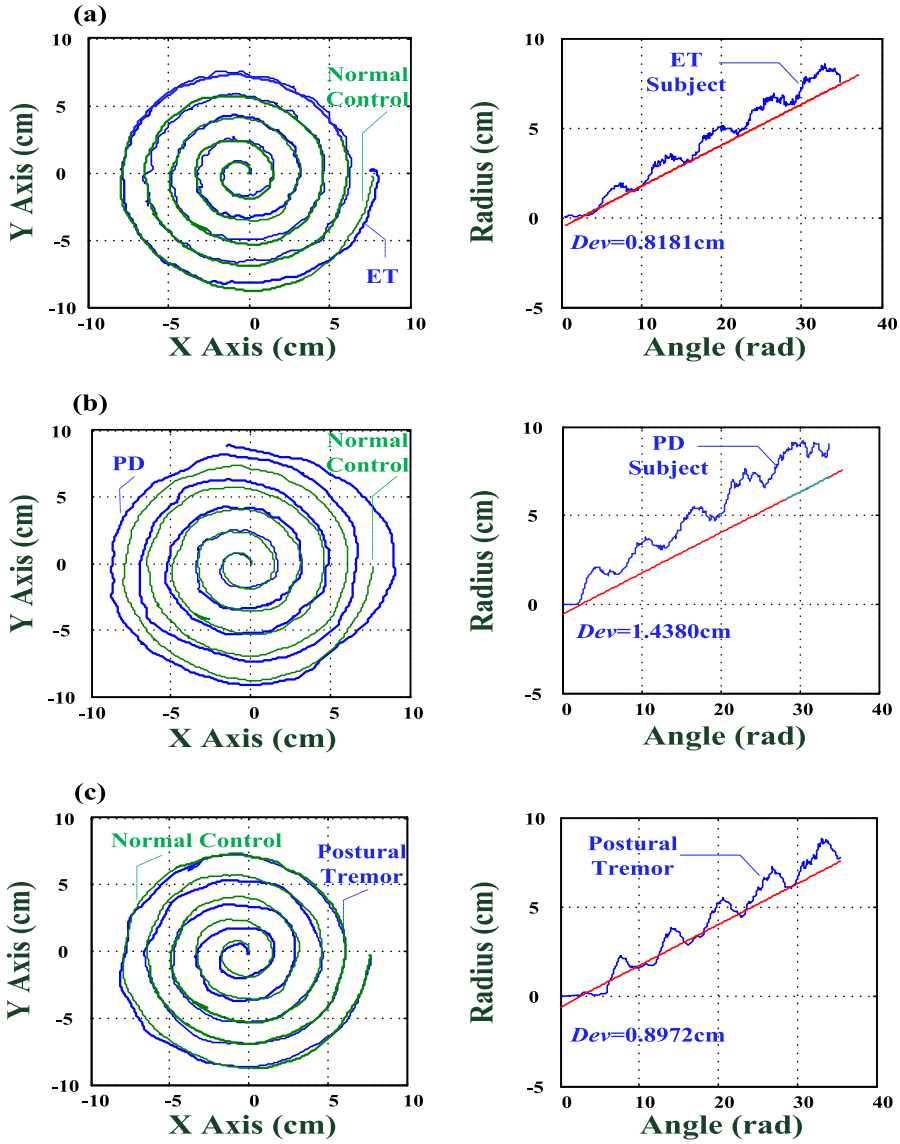

FIGURE 8. Typical handwritten spiral templates for ET, PD, and postural tremor subjects. (a) Spiral template and feature parameter (*Dev* = 0.8181 cm) for ET tremor. (b) Spiral template and feature parameter (*Dev* = 1.4380 cm) for PD tremor. (c) Spiral template and feature parameter (*Dev* = 0.8972 cm) for postural tremor.

Step 1) given the two feature parameters, $[Dev, \Theta] = [0.8154, 7.7541]$,

Step 2) computed 6 certainty grades using equations, (8) – (13), as $[\mu_{Dev,Nor}, \mu_{Dev,ET}, \mu_{Dev,PD}, \mu_{Ang,Nor}, \mu_{Ang,ET}, \mu_{Ang,PD}] = [0.0252, 0.8246, 1.0000, 0.0380, 0.8224, 0.8916]$,

Step 3) used the linguistic inference rules to assign the propositions $[G_1, G_2, G_3, G_4, G_5, G_6]$ and computed the probabilities for 3 classes using equations, (17) – (18), as $[y_1, y_2, y_3] = [0.0175, 0.4573, 0.5252]$,

Step 4) converted the probabilities to the gray grades and converted those to hue angle and saturation using equations, (19)–(23), as $[H, S] = [351.97, 0.9666]$, for red series color to identify the "*PD* case". Index, $S = 0.9666$, offered high confidence to judge the possible severity of PD tremor.

Step 5) normalized the hue angle to lie between 0 and 60 for displayed in computer graphic application.

The entire process took an average CPU time of 0.5301 s to identify the possible class. Furthermore, two expert neurologists agreed with the "PD (Resting Tremor)" level and allowed further medical treatment. These testing results confirmed that the proposed decision support system could separate normal controls from "PD" or "ET" cases, and the saturation index $S \geq 0.5000$, denoted high confidence in this regard. Moreover, for subject #13 (aged 80 years), given the feature parameters, $Dev = 0.8972$ (cm) and $\Theta = 3.4177$ (rad), the screening results indicated "PD" level with indexes $H = 359.47°$ (red) and $S = 0.4552$, and for subject #27 (aged 69 years), given

TABLE 2. Experimental results of fivefold cross validation for PCRC.

Cross Validation	Testing Samples	Testing Samples	True Negative Rate (%)	True Positive Rate (%)	Hit Rate (%)
K_f=1	45: 18 Normal Control, 5 ET, 22 PD	55: 30 Normal Control, 5 ET, 20 PD	90.32 (TN: 28, FP: 3)	91.66 (TP: 22, FN: 2)	90.91 (5 failure)
K_f=2	45: 18 Normal Control, 5 ET, 22 PD	55: 30 Normal Control, 5 ET, 20 PD	90.00 (TN: 27, FP: 3)	88.00 (TP: 22, FN: 3)	89.09 (6 failure)
K_f=3	45: 20 Normal Control, 5 ET, 20 PD	55: 28 Normal Control, 5 ET, 22 PD	89.28 (TN: 25, FP: 3)	88.89 (TP: 24, FN: 3)	89.09 (6 failure)
K_f=4	45: 22 Normal Control, 5 ET, 18 PD	55: 26 Normal Control, 5 ET, 24 PD	88.89 (TN: 24, FP: 3)	92.86 (TP: 26, FN: 2)	90.91 (5 failures)
K_f=5	45: 22 Normal Control, 5 ET, 18 PD	55: 26 Normal Control, 5 ET, 24 PD	92.31 (TN: 24, FP: 2)	93.10 (TP: 27, FN: 2)	92.72 (4 failures)
Average (%)			90.16	90.90	90.54

the feature parameters, $Dev = 0.6249$ (cm) and $\Theta = 8.2187$ (rad), the screening results indicated "ET" level with indexes $H = 291.11°$ (pink) and $S = 0.7304$. Both case studies showed the true positive value for possible level identification with lower confidence. Expert neurologists judged that the participating subjects had postural tremor and Parkinsonism. Postural or action tremor usually occurred in PD, either alone or in combination in the early stage. Seventy percent of PD patients exhibited tremor and had progression of diseases with early postural instability and akinesia. For these cases, the proposed method provided the preliminary diagnosis and then could define the "*warning case*" for continuously monitoring disease progression. In case #31 (aged 74 years), rest tremors might have disappeared during drawing. The proposed decision support system easily allowed subjects to be repeatedly examined in terms of whether they had signs of PD or ET. This confirmed that the proposed decision support system could provide a scientific approach for tremor screening at an early stage. The experimental results for 31 subjects are shown in Table 1.

For untrained patterns as shown in Figure 9, 55 testing patterns were used to validate the PCRC classifier, with a hit rate of 85.45% (8 failures, 4 FPs, and 4 FNs), a true positive rate of 87.88%, and a true negative rate of 81.81% for identifying the correct classes in the recalling stage. In this study, the K-fold cross-validation (rotation estimation) method [30], [31] was also used to evaluate the performance of a classifier model on data of limited size. As general empirical evidence, $K_f = 5$ or 10 was generally performed with interchanging the trained patterns and untrained patterns. In the cross-validation stage, the dataset was divided into two subsets as 45 trained patterns and 55 untrained patterns in each test. In this study, these trained and untrained patterns were randomly selected from dataset for fivefold cross- validation, as seen in Table 2. We started with the subset of data for training purpose and then evaluated the screening accuracy with the untrained patterns, using fivefold cross-validation by separating the testing patterns into five groups. Through fivefold cross-validation, an average true positive rate of 90.90% was obtained to quantify the performance of the proposed classifier for identifying PD or ET, an average true negative rate of 90.16% for identifying normal controls, and an average hit rate of 90.54% for identifying the correct class. The testing data were used to validate classifier feasibility, as seen in Table 2. The results of fivefold cross-validation revealed promising classification capacity from use on limited testing data to estimate the performance of the classifier model.

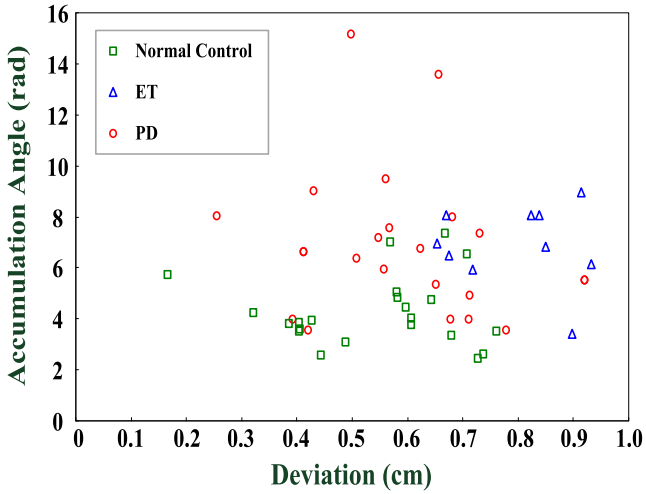

FIGURE 9. Feature Patterns (Dev, Θ) for untrained patterns including normal control, ET, and PD.

B. COMPARISON WITH THE CONVENTIONAL INTELLIGENT CLASSIFIER

The multilayer neural network methods were also selected to train a classifier for separating normal controls from ET or PD cases, such as general regression neural network (GRNN) [32]–[34] and support vector machine (SVM) [35]. To train nonlinearly separable functions, these methods could use the kernel-based function (Gaussian radial basis function) to modify its architecture as a multiclass classifier. The kernel-based transformation transfers the input space into a higher dimensional space through nonlinear transformation. For example, the total number of symptomatic patterns was 45, including 18 for normal controls, 5 for ET, and 22 for PD. We applied the 45 paired input–output training patterns (Dev_k, Θ_k), $k = 1, 2, 3, \ldots, 45$, to determine the GRNN configuration, such as the numbers of inputs, patterns, summations, and output nodes [32]–[34]. The output patterns

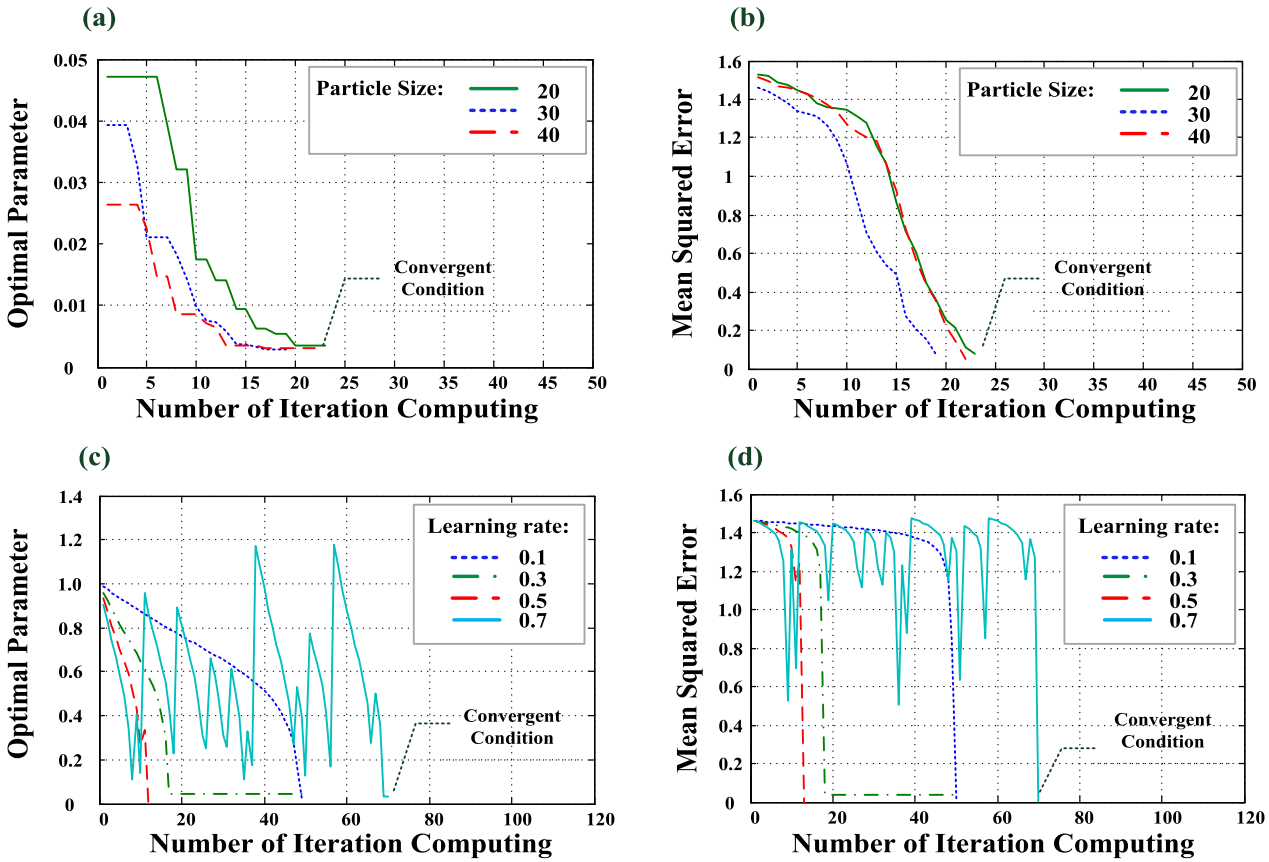

FIGURE 10. Classifier training with the gradient descent and PSO algorithms. (a) and (b) The optimal network parameter and mean squared error versus the number of iteration computing using the PSO algorithm. (c) and (d) The optimal network parameter and mean squared error versus the number of iteration computing using the gradient descent algorithm.

were encoded as binary values with the value "1" or "0" for class identification, as encoding (1) *Class* 1 (normal control): [1, 0, 0], (2) *Class* 2 (ET): [0, 1, 0], and (3) *Class* 3 (PD): [0, 0, 1]. According to the training patterns, we had 2 input nodes, 45 pattern nodes in the hidden layer, 4 nodes in the summation layer, and 3 output nodes (network topology: 2–45–4–3). Two weight matrices, a 45-by-2 matrix and a 45-by-4 matrix, were used to store the connection weights. Considering 4 bytes for each digital storage, the total memory storage was 1080 bytes ($45 \times 2 \times 4$ bytes and $45 \times 4 \times 4$ bytes). Then, the optimization algorithms, such as gradient descent learning algorithm and particle swarm optimization (PSO) algorithm, were used to adjust the optimal network parameter as the width of kernel-based function to minimize the mean squared error (MSE) by iterative computations. The PSO algorithm with time-varying acceleration coefficients [36], [37], different particle sizes, and a maximum iteration number of 50 was carried out to search for the optimal network parameter. We performed at least five runs with the random initial parameters and the given particle sizes, 20–40. For the convergent condition, tolerance value $\leq 10^{-2}$, and a maximum iteration number of 50, the optimal parameters could be guaranteed to minimize the MSE, as seen in Figures 10(a) and 10(b). By increasing the particles from 20 to 40, the solution took <25 iterative computations (average CPU time: 15.98 s) to search for the optimal parameter and the MSE monotonically decreased to reach the convergent condition. For example, a particle size of 30 and optimal network parameter of 0.0035 could be obtained (blue dashed line), and a learning accuracy of 100% was guaranteed in the learning stage.

For the same training patterns, the gradient descent learning algorithm was also used to search for the optimal network parameter with the initial parameter, 1.0000; learning rates, $\eta = 0.1, 0.3, 0.5$, and 0.7; maximum iteration number 100; and convergent condition, $\leq 10^{-2}$. We performed four runs with different learning rates, as seen in Figures 10(c) and 10(d). It could be seen that a greater learning rate, $\eta = 0.7$, allowed a rapid learning stage to search for the optimal parameter. However, its optimal solution was easy to trap the perturbation around the local minimum solution or tend to the divergent condition, as seen from the solid line in Figure 10(d). The optimal solution list could not be guaranteed to reach the convergent condition. The learning accuracy was 75.56% (11 failures) in the learning stage. In addition, with a smaller learning rate, $\eta = 0.1$, its optimal solution list monotonically decreased and was also guaranteed to reach the convergent condition. Its computation took 51 iterative computations (average CPU time: 0.64 s) to determine the optimal parameter, 0.0248, and obtained learning

TABLE 3. Experimental results of fivefold cross-validation for GRNN-based classifier.

Cross-validation	Testing Samples	Testing Samples	True Negative Rate (%)	True Positive Rate (%)	Hit Rate (%)
$K_f = 1$	45: 18 Normal Control, 5 ET, 22 PD	55: 30 Normal Control, 5 ET, 20 PD	90.00 (TN: 27, FP: 3)	88.00 (TP: 22, FN: 3)	89.09 (6 failure)
$K_f = 2$	45: 18 Normal Control, 5 ET, 22 PD	55: 30 Normal Control, 5 ET, 20 PD	87.09 (TN: 27, FP: 4)	87.50 (TP: 21, FN: 3)	87.27 (7 failure)
$K_f = 3$	45: 20 Normal Control, 5 ET, 20 PD	55: 28 Normal Control, 5 ET, 22 PD	88.89 (TN: 24, FP: 3)	85.71 (TP: 24, FN: 4)	87.27 (7 failure)
$K_f = 4$	45: 22 Normal Control, 5 ET, 18 PD	55: 26 Normal Control, 5 ET, 24 PD	82.14 (TN: 23, FP: 5)	88.89 (TP: 24, FN: 3)	85.45 (8 failure)
$K_f = 5$	45: 22 Normal Control, 5 ET, 18 PD	55: 26 Normal Control, 5 ET, 24 PD	84.61 (TN: 22, FP: 4)	86.20 (TP: 25, FN: 4)	85.45 (8 failure)
Average (%)			86.55	87.62	86.91

TABLE 4. Experimental results of fivefold cross-validation for SVM-based classifier.

Cross-validation	Testing Samples	Testing Samples	True Negative Rate (%)	True Positive Rate (%)	Hit Rate (%)
$K_f = 1$	45: 18 Normal Control, 5 ET, 22 PD	55: 30 Normal Control, 5 ET, 20 PD	90.00 (TN: 27, FP: 3)	88.00 (TP: 22, FN: 3)	89.09 (6 failure)
$K_f = 2$	45: 18 Normal Control, 5 ET, 22 PD	55: 30 Normal Control, 5 ET, 20 PD	90.00 (TN: 27, FP: 3)	88.00 (TP: 22, FN: 3)	89.09 (6 failure)
$K_f = 3$	45: 20 Normal Control, 5 ET, 20 PD	55: 28 Normal Control, 5 ET, 22 PD	89.28 (TN: 25, FP: 3)	88.89 (TP: 24, FN: 3)	89.09 (6 failure)
$K_f = 4$	45: 22 Normal Control, 5 ET, 18 PD	55: 26 Normal Control, 5 ET, 24 PD	85.18 (TN: 23, FP: 4)	89.28 (TP: 25, FN: 3)	87.27 (7 failure)
$K_f = 5$	45: 22 Normal Control, 5 ET, 18 PD	55: 26 Normal Control, 5 ET, 24 PD	84.61 (TN: 22, FP: 4)	86.20 (TP: 25, FN: 4)	85.45 (8 failure)
Average (%)			87.81	88.07	87.99

Note: (1) True-positive rate $= (\frac{TP}{TP + FN}) \times 100\%$, where TP and FN are the true positive and false negative, respectively.

(2) True-negative rate $= (\frac{TN}{TN + FP}) \times 100\%$, where TN and FP are true negative and false positive, respectively.

(3) Hit rate $= (\frac{TP + TN}{TP + FN + TN + FP}) \times 100\%$.

accuracy of 100% in the learning stage. As indicated by the red dashed line in Figures 10(c) and 10(d), with learning rate $\eta = 0.5$, the learning stage could rapidly reach the convergent condition in <12 iterative computations (average CPU time: 0.17 s) and also obtained learning accuracy of 100%. The optimal parameter, 0.0071, could also guarantee minimization of the mean squared error. In addition, swarm intelligence algorithm and gradient descent learning algorithm could also be used to train the SVM-based classifier [38].

For the same untrained patterns, 55 testing patterns (22 normal controls, 10 subjects with ET, and 23 subjects with PD) were randomly selected to validate the multilayer neural network method, with a hit rate of 83.63% (9 failures, 5 FPs, and 4 FNs), a true positive rate of 87.50%, and a true negative rate of 78.26%, for identifying the correct class in the recalling stage. The experimental results obtained with the fivefold cross-validations were shown in Tables 3 and 4 for GRNN-based and SVM-based classifiers, as an average true negative rate of 86.55% and 87.81% for identifying normal controls, an average true positive rate of 87.62% and 88.07% for identifying those with PD or ET, and an average hit rate of 86.91% and 87.99% for identifying the correct class, respectively. The multilayer neural network methods offered an adjustable model to train a classifier with input–output paired training patterns in specific applications. To reduce the number of learning computations, the initial conditions and learning parameters were assigned using a trial-and-error method. As feed the new training patterns, its learning process required retraining to adjust the network parameters using the entire datasets. When the number of training patterns was increased, the limitations increased in both the number of iterative computations and the computational time. The convergent condition also affected the training process, reliability, and classification efficiency. In addition, its model required good-quality data, more incremental training patterns, and optimization algorithm efforts to enhance the hit rate, the true positive rate, and the true negative rate. The GRNN and SVM methods had some limitations, including the iterative computations for updating network parameters, initial condition assignment (initial network parameter, acceleration coefficients, learning rate, convergent condition), and network configuration assignment [39].

In contrast to the GRNN and SVM method, the PCRC method had the inference mechanism with perceptual color representations to decision-making in classification application. It is an adaptive pattern mechanism with adjustment of the mean values and standard deviations of membership functions via statistics of current database. Hence, the parameters of membership functions could be directly assigned, which required less parameter assignment and no iterative process to adjust the parameters. In addition, the Bayesian network topological size could be reduced from 2–45–4–3 to 2-6-4.

The memory storage of connection weights could also be reduced from 1080 bytes to 144 bytes ($6 \times 2 \times 4$ bytes and $6 \times 4 \times 4$ bytes). Its model was a visual model to separate the normal control from ET or PD with straightforward mathematical operations. The hue angle used a visual approach with color codes to realize the three levels in green, blue, and red series colors. The PCRC method had the ability to self-regulate the primary color grades using the average gray grades, and minimum and maximum gray grades. This simple decision-making method was easily implemented in a tablet PC and in an intelligent embedded system by commercial HMI (Human Machine Interface) software and C/C++ programming language. This assistant tool also had individualized functions to evaluate the progression of tremor level to meet patient self-care demands.

IV. CONCLUSION

This study developed an assistive tool to screen PD using polar expression features and a perceptual color representation -based intelligent classifier. We intended to offer an automated PD screening method for a computer-aided decision-making system. Digitized handwritten patterns were used to record the dynamics when drawing Archimedes' spirals and straight lines , which could detect movement disorders when any type of tremor occurred. These handwritten patterns showed variability in tremor amplitudes, frequencies, and directions. In polar expression features, two indexes, deviation (Dev) and accumulation angle (Θ), were extracted from the digitized handwritten patterns to scale the variability in different tremor levels, as *Dev* could be quantified in the traced spiral: (1)*normal control*: 0.0464–0.6795 cm, (2) *ET*: 0.5119–1.0651 cm, and (3) *PD*: 0.5009–2.1838 cm; and Θ could be divided into three groups: (1) *normal control*: 2.0766–6.9883 rad, (2) *ET*: 5.9138–14.7004, and (3) *PD*: 5.5155–15.1349 rad. Then, PCRC classifier was employed to separate the normal control from *PD* or *ET* with perceptual color representation, including green series color, blue series color, and red series color. With the fivefold cross-validation, average true positive rate of 92.02%, average true negative rate of 88.68%, and average hit rate of 90.44% were obtained to verify the feasibility of this approach for automated PD screening. In contrast to the multilayer neural network methods, the proposed PCRC method also provided promising results and had higher true positive rate, true negative rate, and hit rate.

The proposed decision support system integrates the iPad and PCRC classifier for individualized functions to evaluate the progression of tremor level and has the following advantages:

- easy acquisition of digitized handwritten patterns using customized software;
- repeated examinations for clinical applications and at-home monitoring uses;
- easy design of an algorithm with less parameter assignment and no iterative process to adjust the network parameters;
- easy implementation of feature extraction and screening algorithms in a portable smart device or a laptop.

In future research, the sensor-based method can be further applied to integrate into the proposed assistive tool. We can also use temporal, spatial, or kinematic parameters of handwriting together with the PCRC classifier or the random decision forest-based classifier (with minimal amounts of parameter tuning) to enhance the classification performance and screening accuracy.

APPENDIX

1. The pseudocodes for replacing the coordinate system are shown below.

Algorithm 1 Pseudocode of Handwritten Spiral Collection for Tremor Analysis

```
% Transform the Archimedes' spiral to origin point
x = x−x(1,1) % Cartesian coordinate system
y = y−y(1,1)
% Convert Pixels to cm
x = 0.19273 + (x ∗ 0.025426)
y = 0.19273 + (y ∗ 0.025426)
% Transform the Cartesian coordinate to polar expression
for i = 1 to N do
    r(1,i) = sqrt((x(1,i)^2) + (y(1,i)^2)) % Radius
    angle(1,i) = abs(atan2(y(i,1),x(i,1))) % Angle
end for
% Angle is a series of increasing or decreasing positive or negative values
for j = 1 to N-1 do
    accumulator = accumulator + abs(angle(1,j) − angle(1,j + 1))
    sum_angle(1,j) = accumulator
end for
% Ideal spiral tracing data for polar expression
for j = 1 to N-1 do
r0(1,i) = (sum_angle(1,j) − 2.5) ∗ (8/35) ;
end for
% Compute the difference between the subject's spiral and ideal spiral
e0 = abs(r − r0)
% Detrend process with the error e0
e1 = detrend(e0)
% Compute the deviation curve
deviation = abs(e0 − e1)
% Compute the slope of deviation curve
slope = abs(deviation(1,1)-deviation (1,n − 1))/sum_angle0(1,n − 1)
% Compute the slope of deviation curve
deviation = slope ∗ sum_angle (1,n − 1)
plot (sum_angle, r0)
plot (sum_angle, deviation)
```

Algorithm 2 Pseudocode of Handwritten Straight Lin for Tremor Analysis

```
% Transform the straight line to origin point
x = x − x(1,1) % Cartesian coordinate system
y = y − y(1,1)
% Convert Pixels to cm
x = 0.19273 + (x ∗ 0.025426)
 y = 0.19273 + (y ∗ 0.025426)
% Transform the Cartesian coordinate to polar expression
for i = 1 to N do
      r0(1,i) = sqrt((x(1,i)^2) + (y(1,i)^2)) % Radius
      angle0(1,i) = abs(atan2(y(i,1),x(i,1))) % Angle
 end for
% Angle is a series of increasing or decreasing positive or negative values
for j = 1 to N − 1 do
      accumulator = accumulator + abs(angle0(1,j) − angle0(1,j + 1))
      sum_angle(1,j) = accumulator
end for
plot (sum_angle, r0)
```

2. Clinical profile of the enrolled subjects.

A total of 100 subjects were enrolled in the IRB project, including normal controls and subjects with ET, PD, and other classes (dementia, muscular rigidity, insomnia, and psychogenic tremors). The profile of the enrolled subjects is shown below.

Overall profile of the enrolled subjects

Class	Normal Control	ET	PD	Other
Subject	40	8	40	12
Gender	23 females, 17 males	5 females, 3 males	19 females, 21 males	5 females, 7 males
Age Range	26–97	43 - 81	56 - 88	53 - 84
Mean Age	62.08 ±17.32	66.00 ±12.61	72.48 ±7.93	70.33 ±9.96

A total of 100 handwritten patterns from 50 subjects were analyzed for early detection application, including 24 normal controls (mean age: 51.25 ± 11.15 years) and 26 subjects with movement disorders, including 5 subjects with ET (mean age: 59.8 ± 6.06 years) and 21 with PD (mean age: 66.52 ± 3.63 years). The grade of disease was age-related, which was confirmed by two expert neurologists. The prevalence of PD increased with advancing age, and it had a tendency to relapse over 60 years of age. ET comprised a slowly progressive monosymptomatic disorder, starting on one side of the body and further affecting both sides and then spreading to the neck and vocal cords within 3 years, with a relapse tendency after 40 years of age. The experimental profile of the enrolled subjects is show' below:

Experimental profile of the enrolled subjects, including normal controls and those with ET and PD

Class	Normal Control	ET	PD	Other
Subject	24	5	21	—
Gender	15 females, 9 males	2 females 3 males	11 females 10 males	—
Age Range	26 - 68	43 - 68	56 - 72	—
Mean Age	51.25 ± 11.15	59.8 ± 6.06	66.52 ± 3.63	—

ACKNOWLEDGMENT

The enrolled data was approved by the hospital research ethics committee and the Institutional Review Board (IRB), under contract number: VGHKS18-CT7-07#, Kaohsiung Veterans General Hospital, Kaohsiung City, Project Leader: Dr. Tsung-Lung Yang, KSVGH Originals & Enterprises, Kaohsiung Veterans General Hospital, Kaohsiung City.

CONFLICT OF INTERESTS

The authors declare that there is no conflict of interests regarding the publication of this paper.

REFERENCES

[1] S. Sveinbjornsdottir, "The clinical symptoms of Parkinson's disease," *J. Neurochem.*, vol. 139, pp. 318–324, Oct. 2016.
[2] M. C. de Rijk *et al.*, "Prevalence of parkinsonism and Parkinson's disease in Europe: The EUROPARKINSON collaborative study. European community concerted action on the epidemiology of Parkinson's disease," *J. Neurology, Neurosurg. Psychiatry*, vol. 62, no. 1, pp. 10–15, 1997.
[3] T. Pringsheim, N. Jette, A. Frolkis, and T. D. Steeves, "The prevalence of Parkinson's disease: A systematic review and meta-analysis," *Movement Disorders*, vol. 29, no. 13, pp. 1583–1590, 2014.
[4] K. C. Brennan, E. C. Jurewicz, B. Ford, S. L. Pullman, and E. D. Louis, "Is essential tremor predominantly a kinetic or a postural tremor? A clinical and electrophysiological study," *Movement Disords*, vol. 17, no. 2, pp. 313–316, 2002.
[5] A. Salarian, H. Russmann, C. Wider, P. R. Burkhard, F. J. G. Vingerhoets, and K. Aminian, "Quantification of tremor and bradykinesia in Parkinson's disease using a novel ambulatory monitoring system," *IEEE Trans. Biomed. Eng.*, vol. 54, no. 2, pp. 313–322, Feb. 2007.
[6] H. Dai, P. Zhang, and T. C. Lueth, "Quantitative assessment of parkinsonian tremor based on an inertial measurement unit," *Sensors*, vol. 15, no. 10, pp. 25055–25071, 2015.
[7] P. Zham, S. P. Arjunan, S. Raghav, and D. K. Kumar, "Efficacy of guided spiral drawing in the classification of Parkinson's disease," *IEEE J. Biomed. Health Inform.*, vol. 22, no. 5, pp. 1648–1652, Sep. 2018.
[8] E.-J. Kim, B.-H. Lee, K. C. Park, W. Y. Lee, and D. L. Na, "Micrographia on free writing versus copying tasks in idiopathic Parkinson's disease," *Parkinsonism Rel. Disorders*, vol. 11, no. 1, pp. 57–63, 2005.
[9] P. Drotár, J. Mekyska, Z. Smékal, I. Rektorová, L. Masarová, and M. Faundez-Zanuy, "Prediction potential of different handwriting tasks for diagnosis of Parkinson's," in *Proc. E-Health Bioeng. Conf.*, Nov. 2013, pp. 1–4.
[10] P. Pierleoni, L. Palma, A. Belli, and L. Pernini, "A real-time system to aid clinical classification and quantification of tremor in Parkinson's disease," in *Proc. IEEE-EMBS Int. Conf. Biomed. Health Inform.*, Valencia, Spain, Jun. 2014, pp. 113–116.
[11] K. Niazmand, K. Tonn, A. Kalaras, U. M. Fietzek, J.-H. Mehrkens, and T. C. Lueth, "Quantitative evaluation of Parkinson's disease using sensor based smart glove," in *Proc. 24th Int. Symp. Comput.-Based Med. Syst.*, Bristol, U.K., Jun. 2011, pp. 1–8.
[12] G. Rigas *et al.*, "Assessment of tremor activity in the Parkinson's disease using a set of wearable sensors," *IEEE Trans. Inf. Technol. Biomed.*, vol. 16, no. 3, pp. 478–487, May 2012.
[13] G. Megali, S. Sinigaglia, O. Tonet, and P. Dario, "Modelling and evaluation of surgical performance using hidden Markov models," *IEEE Trans. Biomed. Eng.*, vol. 53, no. 10, pp. 1911–1919, Oct. 2006.

[14] O. Bazgir, S. A. H. Habibi, L. Palma, P. Pierleoni, and S. Nafees, "A classification system for assessment and home monitoring of tremor in patients with Parkinson's disease," *J. Med. Signals Sensors*, vol. 8, no. 2, pp. 65–72, 2018.
[15] A. Sadikov, J. Zabkar, M. M. Zina, V. Groznik, D. Georgiev, and I. Bratko, "ParkinsonCheck—A decision support system for tremor detection," Semantic Scholar, Tech. Rep., 2015. [Online]. Available: www.ailab.si/parkinsoncheckAQ
[16] D. Miljkovic, D. Aleksovski, V. Podpečan, N. Lavrač, B. Malle, and A. Holzinger, "Machine learning and data mining methods for managing Parkinson's disease," in *Machine Learning for Health Informatics* (Lecture Notes in Computer Science), vol. 9605. Cham, Switzerland, Springer, 2016, pp. 209–220.
[17] S. Lahmiri, D. A. Dawson, and A. Shmuel, "Performance of machine learning methods in diagnosing Parkinson's disease based on dysphonia measures," *Biomed. Eng. Lett.*, vol. 8, no. 1, pp. 29–39, 2018.
[18] S. Lahmiri and A. Shmuel, "Detection of Parkinson's disease based on voice patterns ranking and optimized support vector machine," *Biomed. Signal Process. Control*, vol. 49, pp. 427–433, Mar. 2019.
[19] J. A. Sisti *et al.*, "Computerized spiral analysis using the iPad," *J. Neuroscience Methods*, vol. 275, pp. 50–54, Jan. 2017.
[20] A. P. Legrand *et al.*, "New insight in spiral drawing analysis methods—Application to action tremor quantification," *Clin. Neurophysiol.*, vol. 128, pp. 1823–1834, Oct. 2017.
[21] C. W. Hess, A. W. Hsu, Q. Yu, R. Ortega, and S. L. Pullman, "Increased variability in spiral drawing in patients with functional (psychogenic) tremor," *Hum. Movement Sci.*, vol. 38, pp. 15–22, Dec. 2014.
[22] H.-N. L. Teodorescu, M. Chelaru, A. Kandel, I. Tofan, and M. Irimia, "Fuzzy methods in tremor assessment, prediction, and rehabilitation," *Artif. Intell. Med.*, vol. 21, nos. 1–3, pp. 107–130, 2001.
[23] O. Geman, "A fuzzy expert systems design for diagnosis of Parkinson's disease," in *Proc. E-Health Bioeng. Conf.*, Iasi, Romania, Nov. 2011, pp. 1–4.
[24] C.-H. Lin, "Classification enhancible grey relational analysis for cardiac arrhythmias discrimination," *Med. Biol. Eng. Comput.*, vol. 44, no. 4, pp. 311–320, 2006.
[25] W.-L. Chen, C.-D. Kan, C.-H. Lin, Y.-S. Chen, and Y.-C. Mai, "Hypervolemia screening in predialysis healthcare for hemodialysis patients using Fuzzy color reason analysis," *Int. J. Distrib. Sensor Netw.*, vol. 13, no. 1, pp. 1–13, Jan. 2017.
[26] W.-L. Chen, C.-D. Kan, and C.-H. Lin, "Assessment of inflow and outflow stenoses using big spectral data and radial-based colour relation analysis on *in vitro* arteriovenous graft biophysical experimental model," *IET Cyber-Phys. Syst., Theory Appl.*, vol. 2, no. 1, pp. 10–19, Apr. 2017.
[27] W.-L. Chen *et al.*, "Assistive technology using regurgitation fraction and fractional-order integration to assess pulmonary valve insufficiency for pre-surgery decision making and post-surgery outcome evaluation," *Biomed. Signal Process. Control*, vol. 44, pp. 247–257, Jul. 2018.
[28] *Detrend*. Accessed: 2019. [Online]. Available: https://www.mathworks.com/help/matlab/ref/deterndhtml#syntax
[29] MathWorks, Inc. *MATLAB Data Analysis*. Accessed: 2019. [Online]. Available: https://www.Mathworks.com/help/pdf_doc/matlab/data_analysis.pdf
[30] M. Ljumović and M. Klar, "Estimating expected error rates of random forest classifiers: A comparison of cross-validation and bootstrap," in *Proc. 4th Medit. Conf. Embedded Comput.*, Jun. 2015, pp. 212–215.
[31] M. Al Helal, M. S. Haydar, and S. Al Mahmud Mostafa, "Algorithms efficiency measurement on imbalanced data using geometric mean and cross validation," in *Proc. Int. Workshop Comput. Intell.*, Dec. 2016, pp. 110–114.
[32] D. F. Specht, "A general regression neural network," *IEEE Trans. Neural Netw.*, vol. 2, no. 6, pp. 568–576, Nov. 1991.
[33] C.-H. Lin, C.-D. Kan, J.-N. Wang, W.-L. Chen, and P.-Y. Chen, "Cardiac arrhythmias automated screening using discrete fractional-order integration process and meta learning based intelligent classifier," *IEEE Access*, vol. 6, pp. 52652–52667, 2018.
[34] C.-D. Kan *et al.*, "Customized handmade pulmonary valved conduit reconstruction for children and adult patients using meta-learning based intelligent model," *IEEE Access*, vol. 6, pp. 21381–21396, 2018.
[35] P. Drotár, J. Mekyska, I. Rektorová, L. Masarová, Z. Smékal, and M. Faundez-Zanuy, "Decision support framework for Parkinson's disease based on novel handwriting markers," *IEEE Trans. Neural Syst. Rehabil. Eng.*, vol. 23, no. 3, pp. 508–516, May 2015.
[36] A. Ratnaweera, S. K. Halgamuge, and H. C. Watson, "Self-organizing hierarchical particle swarm optimizer with time-varying acceleration coefficients," *IEEE Trans. Evol. Comput.*, vol. 8, no. 3, pp. 240–255, Jun. 2004.
[37] T.-H. S. Li *et al.*, "A three-dimensional adaptive PSO-based packing algorithm for an IOT-based automated e-fulfillment packaging system," *IEEE Access*, vol. 5, pp. 9188–9205, 2017.
[38] C.-M. Li *et al.*, "Synchronizing chaotification with support vector machine and wolf pack search algorithm for estimation of peripheral vascular occlusion in diabetes mellitus," *Biomed. Signal Process. Control*, vol. 9, pp. 44–55, Jan. 2014.
[39] A. Holzinger, "From machine learning to explainable AI," in *Proc. World Symp. Digit. Intell. Syst. Mach. (DISA)*, Aug. 2018, pp. 55–66.

PING-JU KAN was born in Tainan, Taiwan, in 1998. He moved to Canada, in 2010. He started studying computer science at the University of Toronto, ON, Canada, in 2016. His grade point average in school is 3.92/4.0.

As his parents work as medical staffs, he also grew an interest in health information field. In 2018, not subject to his studentship, the Kaohsiung Veterans General Hospital Originals and Enterprises Center took a liking to his ability and provided him an adjunct position. He worked for the projects, including computerized spiral analysis using iPad and Apple pencil, exploring the application of additive manufacturing in the clinical treatment of wrist disorders, and others. Continuously, he works oversea and study hard at the same time. His research interests include algorithms, probability, machine learning, data structures, numerical analysis, and artificial intelligence.

CHIA-HUNG LIN was born in Kaohsiung, Taiwan, in 1974. He received the B.S. degree from the Tatung Institute of Technology, Taipei, Taiwan, in 1998, and the M.S. and Ph.D. degrees from National Sun Yat-sen University, Kaohsiung, in 2000 and 2004, respectively, all in electrical engineering.

He was a Professor with the Department of Electrical Engineering, Kao-Yuan University, Kaohsiung, from 2004 to 2017. Since 2018, he has been a Professor with the Department of Electrical Engineering and a Researcher with the Artificial Intelligence Application Research Center, National Chin-Yi University of Technology, Taichung, Taiwan. His research interests include neural network computing and its applications, biomedical signal and image processing, healthcare, hemodynamic analysis, and pattern recognition.

CHEN-SAN SU was born in Kaohsiung, Taiwan, in 1975. She received the M.D. degree from the Department of Medicine, Kaohsiung Medical University, Taiwan, in 2000.

After had graduated from the university, she received full neurology resident training at Chang-Gung Memorial Hospital, one of the medical centers in Taiwan. She has been a Board Certified Neurologist, since 2003, and she has been an Attending Staff, since 2005. She is currently a specialist with the Kaohsiung Veterans General Hospital, Kaohsiung. Her specialty and research interest include movement disorders and sleep disorders.

HSIN-YU LIN was born in Kaohsiung, Taiwan, in 1992. She was graduated from the Nursing Department, Kaohsiung Medical University, Taiwan. She is currently pursuing the master's degree in visual design with National Kaohsiung Normal University, Kaohsiung.

She was with the Changhua Christian Hospital and the Kaohsiung Veterans General Hospital as a Nurse. She became a Staff of the Kaohsiung Veterans General Hospital Originals and Enterprises Center, Kaohsiung. Her research interests include nursing and visual design.

WEI-LING CHEN was born in Kaohsiung, Taiwan, in 1970. She received the B.S. degree in mechanical engineering, the M.S. degree in biomedical engineering, and the Ph.D. degree in biomedical engineering from National Cheng Kung University, Tainan, Taiwan, in 1994, 1996, and 2015, respectively.

She is currently with the Department of Engineering and Maintenance, Kaohsiung Veterans General Hospital, Kaohsiung, in 2013, where she has been with KSVGH Originals and Enterprises, since 2018. She has also been an Assistant Professor with the Department of Nursing, Mei-Ho University, Pingtung, Taiwan, since 2018. Her research interests include biomedical signal processing, hemodynamic analysis, healthcare, numerical analysis, medical device design, and numerical analysis.

CHIH-KUANG LIANG was born in 1974. He received the M.D. degree from the School of Medicine, National Yang-Ming University, Taipei, Taiwan, in 2000.

He got the National Board of Internal Medicine, in 2004, and Neurology, in 2007. He has also been an Assistant Professor with the School of Medicine, National Yang-Ming University, since 2016. He is currently the Chief of the Division of Geriatric Medicine, Center for Geriatrics and Gerontology, Kaohsiung Veterans General Hospital, Kaohsiung, Taiwan. His research interests include geriatric medicine, frailty, sarcopenia, neurodegenerative disorders, dementia, and healthcare.